




Research Article



Characterization of Scour-Induced Subsurface Deformations in Port Structures with Contiguous Pile Walls using Ground-Penetrating Radar (GPR)

Navid Joushideh^{1*} , Amin Majidi², Hamid Tabrizi³, Sara Shomal Zadeh³

¹ Department of Civil Engineering, University of Memphis, 3720 Alumni Ave, Memphis, TN 38152, United States

² Department of Civil Engineering, University of Mohaghegh Ardebili, Ardebil, Iran

³ Department of Civil and Environmental Engineering, Lamar University, Beaumont, TX 77710, United States

Keywords

Ground penetration radar,
Quay wall,
Pile groups,
Non-destructive testing,
subsurface.

Abstract

This study presents a comprehensive investigation of subsurface manifestations, including potential cavities and scouring phenomena, within Berths 1 to 9 of Bandar-e-Anzali port, Iran, utilizing ground-penetrating radar (GPR) surveys. The objective of the study was to gain insights into the prevailing subsurface conditions and identify any critical situations that could lead to settlement and collapse, particularly related to scour-induced cavities. A total of 94 profiles were obtained using a GPR device equipped with a 250 MHz antenna, covering approximately 1,400 meters of the quay length. The collected data underwent various processing techniques, including background removal, Fk filter, contrast adjustment, and gain adjustment. Analysis and interpretation of the data revealed anomalies beneath the quay, primarily near the piles of the quay wall and beneath the utility trenches. Test pits were excavated at specific points to verify the accuracy of the results, confirming significant void spaces and cavities exceeding depths of 1.5 meters. These findings indicate a susceptibility to settlement and collapse due to water penetration and scouring of materials in close proximity to the sea. The study highlights the importance of GPR surveys in assessing subsurface conditions and identifying potential risks in marine structures such as ports and jetties.

1. Introduction

Pile groups are commonly used in marine structures such as jetties, seawalls, and offshore structures. The stability of these piles can be significantly affected by scour, which is the erosion of sediment around the pile. However, compared to scour around bridge piers in rivers or canals, there is limited research available on scour around marine structures [1-9].

Scouring can occur in areas that are not easily accessible or visible, such as beneath port docks. In port areas with its bustling environment and heavy traffic, traditional in-situ penetration tests are often impractical and can cause damage

to pavements and underground utilities. As a result, non-destructive geophysical survey methods, including Ground Penetrating Radar (GPR), have gained popularity [10].

Ground Penetrating Radar (GPR) has emerged as a non-destructive geophysical technique that provides high-resolution subsurface imaging. Since its introduction in the 1970s, GPR has been successfully applied worldwide for the detection and mapping of subsurface features [11]. By utilizing high-frequency electromagnetic waves, GPR offers a rapid and continuous method for investigating near-subsurface structures [12]. The principle of GPR is based on the ability of radar waves and microwaves to penetrate the subsurface, with the depth of penetration depending on the

* Corresponding Author: Navid Joushideh

E-mail address: njshideh@memphis.edu, ORCID: <https://orcid.org/0009-0008-1276-3917>

Received: 20 May 2023; Revised: 12 June 2023; Accepted: 17 June 2023

<https://doi.org/10.61186/crpase.9.2.2847>

Academic Editor: Vahid Najafi Moghadam Gilani

Please cite this article as: N. Joushideh, A. Majidi, H. Tabrizi, S. Shomal Zadeh, Characterization of Scour-Induced Subsurface Deformations in Port Structures with Contiguous Pile Walls using Ground-Penetrating Radar (GPR), Computational Research Progress in Applied Science & Engineering, CRPASE: Transactions of Civil and Environmental Engineering 9 (2023) 1–8, Article ID: 2847.

signal frequency and electromagnetic properties of the medium [13]. It involves transmitting electromagnetic waves into the subsurface and monitoring their reflections and refractions upon return to the ground surface [14]. Unlike seismic exploration, which uses sound waves, GPR utilizes electromagnetic waves to detect discontinuities in the subsurface, primarily the electrical properties such as relative dielectric permittivity.

GPR surveys have found applications in various fields, such as structural health monitoring, underground mapping, and geological structure investigations [15-18]. Combining GPR with other survey techniques, such as standard penetration tests and falling weight reflectometry, has proven beneficial in overcoming the limitations of GPR and evaluating subsurface layers more effectively [19].

In geotechnical and structural applications, GPR has proven to be a valuable tool for imaging reinforcing bars, voids, tendon ducts in concrete structures, and identifying subsurface voids beneath concrete roads [20-27].

The choice of GPR frequency depends on the specific application and desired field of investigation. Frequencies ranging from 10 MHz to 2 GHz have been used for diverse purposes, including oil and gas exploration, mineral and groundwater exploration, geology, subsurface utility detection, and geotechnical and archaeological investigations [28-31]. GPR has been widely employed to characterize subsurface cavities, detect utilities, provide information on subsurface layers and properties, and explore karst systems and archaeological sites [32-35].

This study utilized GPR surveys to comprehensively investigate subsurface manifestations, including potential cavities and scouring phenomena, within Berths 1 to 9 of Bandar Anzali port, Iran. The main objective was to gain insights into the prevailing subsurface conditions and determine if any critical situations exist that could potentially lead to settlement and collapse, particularly in relation to scour-induced cavities. By conducting thorough analysis and interpretation of the collected GPR data, the study aimed to identify and evaluate any areas at risk of such hazardous conditions.

2. GPR Principles

Ground-penetrating radar (GPR) is an electromagnetic pulse reflection method that shares similarities with reflection seismic in terms of its underlying physical principles. It has emerged as a high-resolution geophysical technique for shallow investigations and has experienced significant advancements in the past few decades. Throughout its development, GPR has been referred to by various synonyms and acronyms, such as electromagnetic reflection (EMR), subsurface interface radar (SIR), georadar, subsurface penetrating radar, and soil radar. Its roots can be traced back to the 1960s when it was initially used as radio echo sounding (RES) for measuring ice thickness on polar ice sheets. The method was pioneered by STERN (1929, 1930) in Austria to estimate glacier thickness.[35]

Since the 1980s, GPR has gained increasing acceptance in various fields, including geology, engineering, environmental studies, and archaeology. In its basic time-

domain form, GPR involves transmitting electromagnetic pulses into the ground. A portion of this energy is reflected or scattered at boundaries between different rock strata or buried objects. The direct and reflected amplitudes of the electric field strength (E) are recorded as a function of travel time [36].

The potential advantage of GPR lies in its non-destructive nature for subsurface mapping. This method eliminates the need for exploratory drilling or soil disturbance, which are costly, time-consuming, and fundamentally destructive to the sampled area and its information. In addition, GPR surveys are faster and more economical, providing higher spatial accuracy compared to other conventional methods. This method has the capability of obtaining subsurface information from depths ranging from a few centimeters to several meters.

3. Wave Propagation, Velocity, and Absorption

The propagation of electromagnetic waves has a greater dependence on the wave frequency compared to sound waves. This frequency dependency results in changes in the shape of the transmitted pulse during the process of propagation, reflection, and refraction from different interfaces. The electric field component of a plane wave propagating in the Z direction (depth) is defined as Eq. (1) [37]

$$E(t, z) = E_0 e^{(i\omega t - \gamma z)} [Vm^{-1}] \quad (1)$$

In Eq. (1), E represents the electric field and ω is the angular frequency. The magnetic field component of electromagnetic waves is perpendicular to the electric field component and perpendicular to the propagation direction. The electromagnetic wave inside the ground moves downward in a three-dimensional cone shape.

The velocity of the propagated electromagnetic wave within the ground can be obtained from Eq. (2)

$$V = \frac{C_0}{\sqrt{\epsilon'_r \mu'_r \frac{1 + \sqrt{1 + (\frac{\sigma}{\epsilon' \omega})^2}}{2}}}} \quad (2)$$

In Eq. (2), C_0 is the speed of light in vacuum, μ'_r is the real part of the relative permeability, ϵ'_r is the imaginary part of the relative permeability, and ω is the angular frequency of the GPR wave. In low-loss media, the term $\frac{\sigma}{\epsilon' \omega}$ approaches zero. Additionally, if μ'_r is small in non-magnetic media, it can be approximated to one. Thus, we have [38-40]:

$$V = \frac{C_0}{\sqrt{\epsilon'_r}} \quad (3)$$

It should be noted that Eq. (3) is not valid for materials with high conductivity such as seawater, certain types of clays, and magnetic materials like magnetite and hematite. The electromagnetic properties of different materials, including relative permittivity, conductivity, velocity, and wave attenuation in various media, are listed in Table 1.

Table 1. Relative permittivity ϵ'_r , electric conductivity σ , velocity v , and absorption coefficient α' of several materials [36]

Material	ϵ'_r [dimensionless]	σ [mSm ⁻¹]	v [m ns ⁻¹]	α' [dB m ⁻¹]
Air	1	0	0.2998	0
Distilled water	80	0.01	0.033	0.002
Fresh water	80	0.5	0.033	0.1
Sea water	80	0	0.01	1000
Dry sand	3–5	0.01	0.15	0.01
Water-saturated sand	20–30	0.1–1	0.06	0.03–0.3
Silt	5–30	1–100	0.07	1–100
Clay	5–40	2–1000	0.06	1–300
Limestone	4–8	0.5–2	0.12	0.4–1
Shale	5–15	1–100	0.09	1–100
Granite	6	0.01–1	0.12	0.01–1
Dry salt	≈ 6	0.001–0.1	0.125	0.01–1
Ice	3.18	0.01	0.168	0.02
Oil, asphalt	2–3	0.01	0.19	0.01

The electromagnetic properties of a dielectric can also be described by the complex characteristic impedance Z^* (the ratio of electric to magnetic field strength):

$$Z^* = Z' + iZ'' = \sqrt{\frac{\mu^*}{\epsilon^*}} \quad (4)$$

where μ^* is the complex magnetic permeability and ϵ^* is the complex permittivity.

At the boundary between two media with different electrical properties, an arriving electromagnetic wave is both reflected and refracted. A portion of the incident wave energy is reflected back, while another portion passes through the common interface and penetrates into the second medium. The reflection coefficient and transmission coefficient are expressed by Eq. (5) and Eq. (6) [36]

$$r = \frac{Z_2 \cos \phi - Z_1 \cos \psi}{Z_2 \cos \phi + Z_1 \cos \psi} \quad (5)$$

$$t = \frac{2Z_2 \cos \phi}{Z_2 \cos \phi + Z_1 \cos \psi} \quad (6)$$

where ϕ is the angle of incidence, ψ is the angle of refraction, v_1 and v_2 are the wave velocities in the two media, and Z_1 and Z_2 are the electrical wave impedances. When the incidence is perpendicular to the boundary plane (i.e., $\psi = \phi = 90^\circ$), Eq. (5) reduces to:

$$r = \frac{Z_2 - Z_1}{Z_2 + Z_1} \quad (7)$$

which under low loss conditions ($\tan \delta \ll 1$ and $\mu_i^* \approx \mu_0$) can be expressed as:

$$r \cong \frac{\sqrt{\epsilon'_{r1}} - \sqrt{\epsilon'_{r2}}}{\sqrt{\epsilon'_{r1}} + \sqrt{\epsilon'_{r2}}} \cong \frac{v_2 - v_1}{v_2 + v_1} \quad (8)$$

Because the impedances Z_i are complex values Eq. (4), r and t are also complex, even for incident waves perpendicular to the boundary plane. Reflection and transmission of electromagnetic waves at the boundary between two strata with different electrical properties (i.e., there is a change in $\tan \delta$) always involves deformation of the wavelet Figure 1. This is a significant difference from reflection seismics.

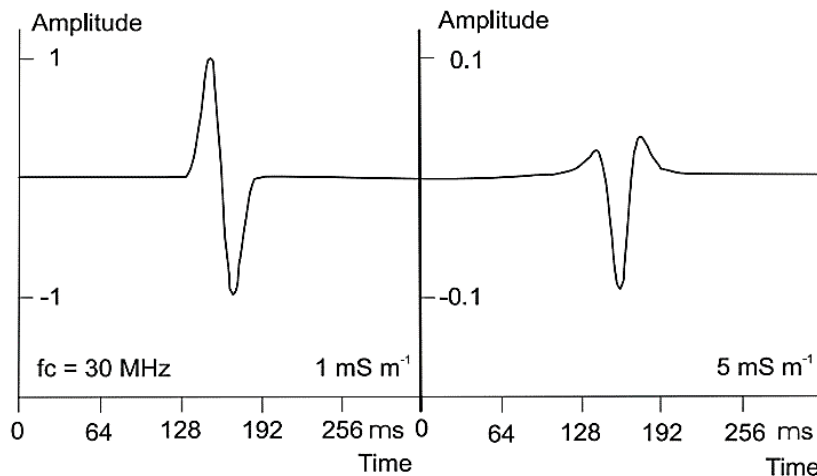


Figure 1. Wavelet before (left) and after (right) perpendicular reflection at a boundary plane at which the conductivity changes from 1 to 5 mS m⁻¹ [36].

When incident to boundaries, electromagnetic waves behave in a complicated geology (e.g., thin layers, lamellae, gradient zones) similarly to seismic waves. Multiple reflections at the ground surface are not significant for GPR,

because there is usually considerable absorption by the soil and rock and only up to about 10 % of the transmitted energy is reflected by the ground surface [36].

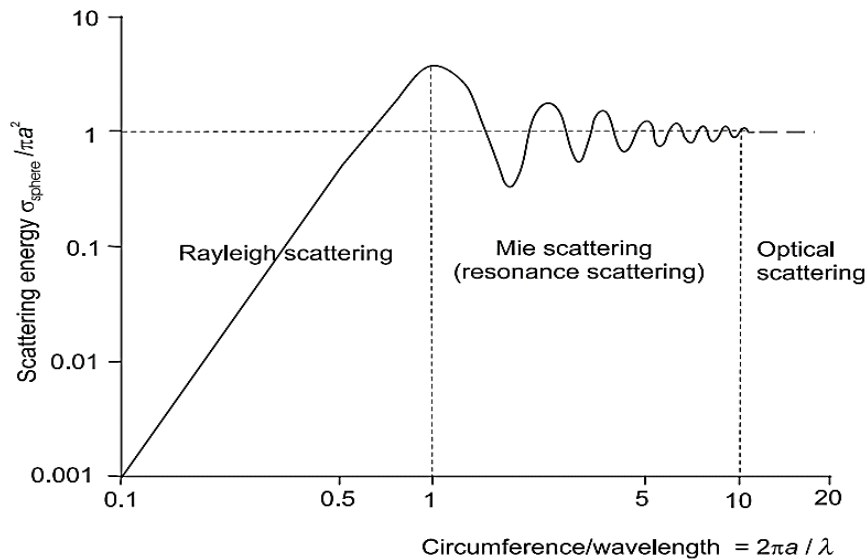


Figure 2. Scattering from a conductive sphere with a radius α [36].

4. Penetration Depth

The penetration depth in GPR is controlled by the central frequency and the attenuation coefficient of the subsurface structures, which is a function of their electrical conductivity [41]. In low-loss media, lower-frequency antennas penetrate to relatively greater depths, while higher-frequency antennas penetrate to shallower depths. This indicates an inverse relationship between penetration depth and the central frequency of GPR waves. Research reports based on sedimentology show that the penetration depth for frequencies ranging from 40 to 50 MHz is 30 to 40 meters, for 100 MHz it is 10 to 25 meters, for 200 MHz it is 5 to 15 meters, and for frequencies of 500 to 1000 MHz, it is only a few meters. The maximum penetration depth achieved by GPR waves has been observed in dry rocks, dry sand, and pure sand deposits [41-44].

The propagation of waves inside the ground leads to energy loss. The rate of signal attenuation in GPR is simply dependent on the electrical conductivity of the ground. Materials with high electrical resistivity (insulating materials) result in weaker signal strength with lower velocities. On the other hand, in materials with high conductivity, such as clayey soil or deposits filled with saline water pathways, rapid attenuation occurs, significantly reducing the penetration depth. For example, using a 100 MHz GPR antenna in clayey deposits, the penetration depth is only a few meters, whereas in deposits filled with saline water pathways, the penetration depth is reduced to a few centimeters.

5. GPR Data Processing

In general, geophysical data processing is carried out to overcome inherent limitations and noise present in raw data. The GPR method is no exception, and even in some studies, achieving the desired target without applying appropriate processing techniques may seem impossible. The range of processing techniques applied to the data is controlled by various parameters.

In some studies, initial data processing may be avoided, and a wide range of processing techniques can be applied to the data. Typically, in the first stage, the data undergo editing processes. These processes include zero-time correction, flipping the profile direction, file merging, removal of duplicate traces, and adding them to the stations where the acquisition took place. Editing of acquisition parameters such as center frequency and antenna spacing is also carried out during this stage.

In the next stage of data editing, appropriate filters are applied to remove noise. Finally, due to the attenuation and geometric spreading of electromagnetic waves, reflections at greater depths become much weaker.

6. Site Characterization

The study site is situated in Bandar Anzali Port, which is located on the southern coast of the picturesque Caspian Sea in Gilan Province, Iran (Figure 3). The structural system employed in the quay of Bandar-e Anzali Port consists of a contiguous pile wall, which is divided into 10 berths, with a total length of approximately 1400 meters. Berths 5 and 6 are constructed using concrete piles, while the remaining berths utilize steel piles that are filled with concrete.



Figure 3. location of study site in Bandar-e-Anzali Port, north of Iran.

The piles in berths 5 and 6 are precast concrete piles with a circular cross-section measuring 100 centimeters in diameter. On the other hand, the piles in berths 1 to 4 and 7 to 10 are steel piles filled with concrete, featuring a diameter of 75 centimeters and a wall thickness of 2.9 millimeters. Within the piles, reinforced concrete is implemented starting

from an elevation of -10.25 meters, and this reinforced concrete core is fully connected to the slab. The elevation of the pile foot is -17.25 meters, and the length of the piles is approximately 18 meters. For a visual representation, please refer to Figure 4 and 5, which depicts the plan of the piles.

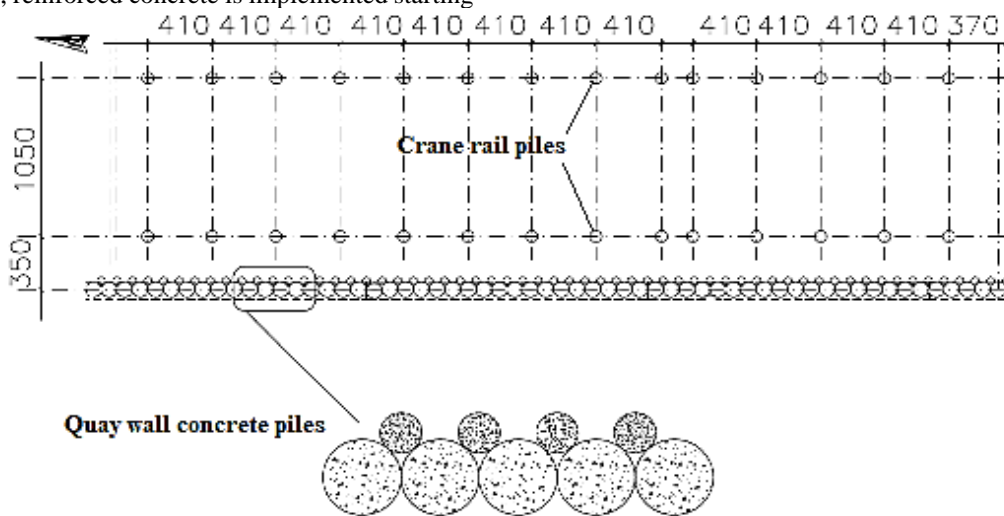


Figure 4. Bandar-e-Anzali port's contiguous piles quay wall plan view

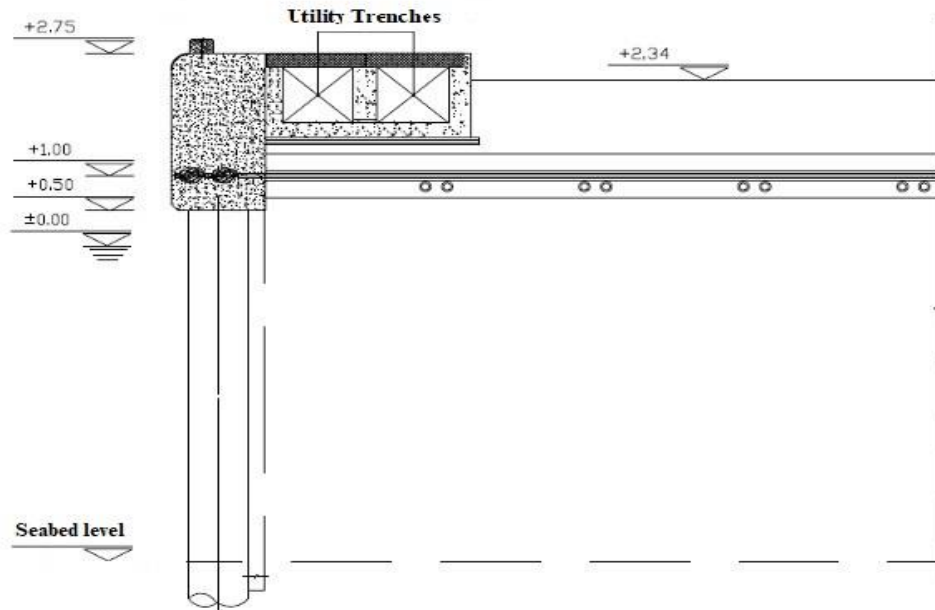


Figure 5. Cross section view of quay wall, berth 5, Bandar-e-Anzali Port, Iran

Over time, the action of water currents in the sea and its impact on the quay's piles have resulted in the deterioration of pile materials and the formation of gaps between them. This has led to the penetration of water beneath the quay's slab and the subsequent washout of existing materials, as well as the development of scouring induced cavities.

7. Data Analysis and Discussion of Results

Approximately 1,400 meters of quay length were surveyed in two lines, starting from berth 1 to berth 10. A total of 94 profiles were obtained using a GPR device

equipped with a 250 MHz antenna mounted on an RTC cart. The velocity of electromagnetic waves within the materials present in the study area was assumed to be approximately 82 m/μs, following ASTM D6432 standard [45]. The maximum penetration depth of the 250 MHz antenna was 8 meters. Data processing techniques such as background removal, Fk filter, contrast adjustment, and gain adjustment were applied to the collected data. Some of the obtained radargram profiles are illustrated in Figure 6. The identified anomalies' positions are indicated on their respective radargrams, allowing for easy geometric extraction of their locations.

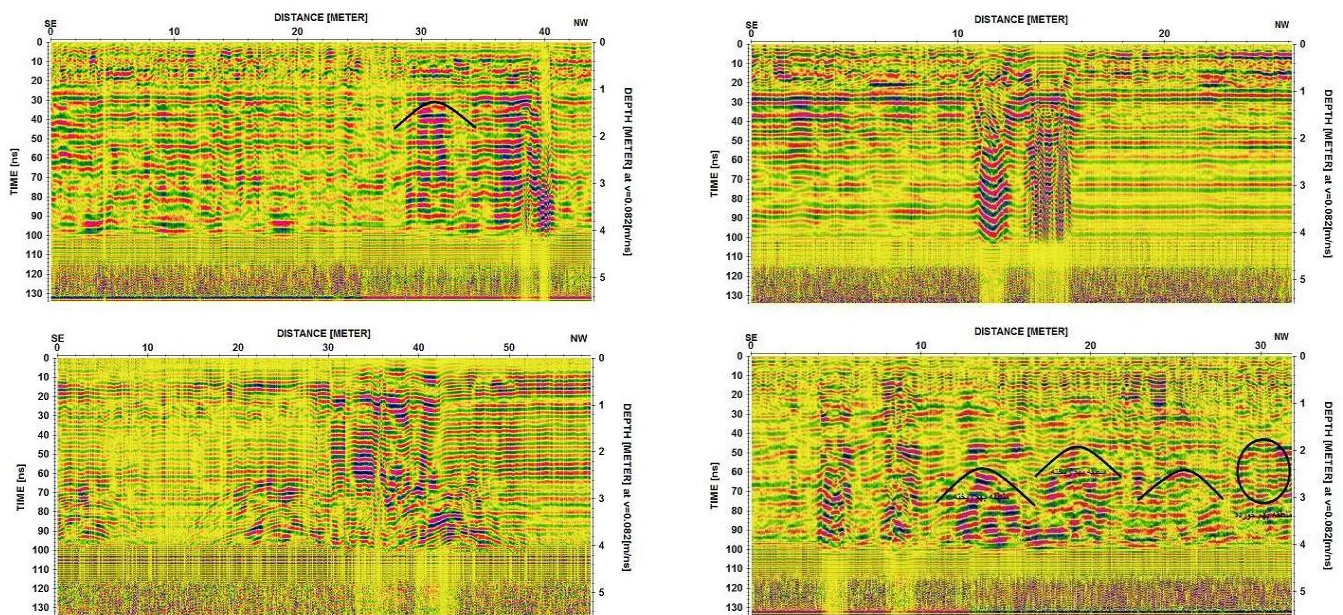


Figure 6. Some of the GPR radargram collected with 250 MHz antenna along survey lines.

After processing the collected radargram profiles and analyzing and interpreting the data, anomalies were identified beneath the quay, particularly near the piles of the

quay wall and beneath the utility trenches. The positions and density of these anomalies along the quay are depicted in Figure 7.

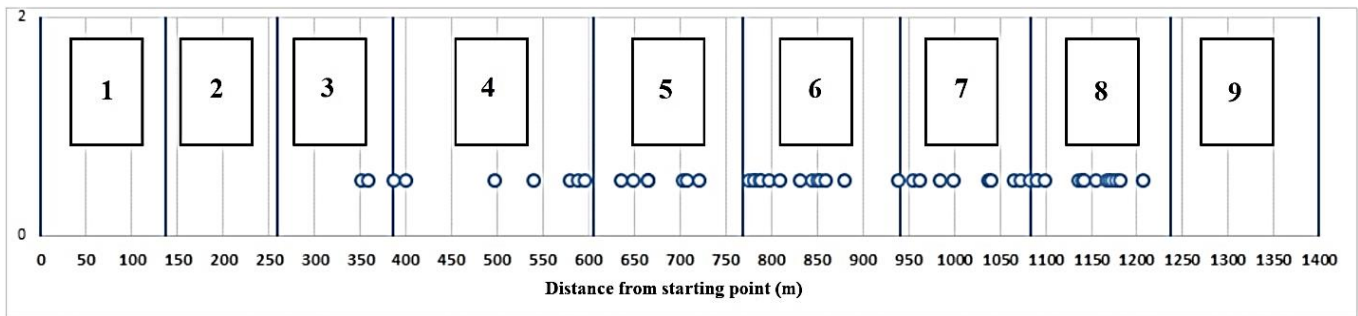


Figure 7. The distribution of anomalies along the quay length

To further validate the accuracy of the obtained results, excavation of test pits was carried out at specific locations behind the utility trenches, reaching depths ranging from approximately half a meter to two meters. Notably, these excavations revealed significant void spaces beneath the utility trenches, with some cavities exceeding depths of 1.5 meters. These findings provided confirmation of the observations made during the ground-penetrating radar (GPR) surveys.

Based on the conducted surveys, it was determined that the extent of these cavities was substantial, primarily encompassing the area between the utility trenches and the cap beam, spanning a width of approximately 2 to 3 meters. This phenomenon was predominantly observed along the entire length of berths 5, 6, 7, and 8, with certain areas of berths 3 and 4 also exhibiting similar effects.

The observed anomalies, which are located in close proximity to the sea, are believed to be the outcome of water infiltration between the piles and the scouring of materials, rendering them vulnerable to settlement and collapse.

Furthermore, it is noteworthy to mention that the GPR survey results were found to be in agreement with 93% of the actual cavities detected during the excavation, further demonstrating the reliability and effectiveness of the GPR method in accurately identifying subsurface anomalies.

7. Conclusion

In conclusion, the study conducted a thorough investigation of subsurface manifestations in Berths 1 to 9 of Bandar-e-Anzali port, Iran, using ground-penetrating radar (GPR) surveys. Analysis of the data revealed significant void spaces and cavities exceeding depths of 1.5 meters, primarily near the piles of the quay wall and beneath the utility trenches. The study found that approximately 93% of the surveyed area exhibited subsurface anomalies, indicating a high susceptibility to settlement and collapse. These findings highlight the critical role of GPR surveys in identifying potential risks and guiding maintenance efforts to prevent further deterioration and ensure the long-term stability of port structures.

References

[1] Y. Mostafa, Associate, A. Agamy, Assistant, SCOUR AROUND SINGLE PILE AND PILE GROUPS

- SUBJECTED TO WAVES AND CURRENTS, International Journal of Engineering Science and Technology 3 (2011).
- [2] B.W. Melville, Y.-M. Chiew, Time Scale for Local Scour at Bridge Piers, *Journal of Hydraulic Engineering* 125(1) (1999) 59–65.
- [3] B.W. Melville, A.J. Sutherland, Design Method for Local Scour at Bridge Piers, *Journal of Hydraulic Engineering* 114(10) (1988) 1210–1226.
- [4] A.J. Raudkivi, R. Ettema, Effect of Sediment Gradation on Clear Water Scour, *Journal of the Hydraulics Division* 103(10) (1977) 1209–1213.
- [5] B.M. Sumer, R.J.S. Whitehouse, A. Tørum, Scour around coastal structures: a summary of recent research, *Coastal Engineering* 44 (2001) 153–190.
- [6] B.M. Sumer, K. Bundgaard, J. Fredsøe, Global and local scour at pile groups, *International Journal of Offshore and Polar Engineering* 15(3) (2005) 204–209.
- [7] B.M. Sumer, J. Fredsøe, Wave Scour around Group of Vertical Piles, *Journal of Waterway, Port, Coastal, and Ocean Engineering* 124(5) (1998) 248–256.
- [8] B.M. Sumer, J. Fredsøe, Scour around Pile in Combined Waves and Current, *Journal of Hydraulic Engineering* 127 (2001) 403–411.
- [9] M.S. Alasta, A.S.A. Ali, S. Ebrahimi, M.M. Ashiq, A.S. Dheyab, A. AlMasri, A. Alqatanani, M. Khorram, Modeling of local scour depth around bridge pier using FLOW 3D, *CRPASE: Transactions of Civil and Environmental Engineering* 8(2) (2022) 1–9.
- [10] M. van Schoor, Detection of sinkholes using 2D electrical resistivity imaging, *Journal of Applied Geophysics* 50(4) (2002) 393–399.
- [11] J.L. Davis, A.P. Annan, GROUND-PENETRATING RADAR FOR HIGH-RESOLUTION MAPPING OF SOIL AND ROCK STRATIGRAPHY1, *Geophysical Prospecting* 37(5) (1989) 531–551.
- [12] M. Clark, M. Gordon, M.C. Forde, Issues over high-speed non-invasive monitoring of railway trackbed, *NDT & E International* 37(2) (2004) 131–139.
- [13] D.J. Daniels, *Ground Penetrating Radar*, Institution of Engineering and Technology 2004.
- [14] G. Valerio, A. Galli, P. Matteo Barone, S.E. Lauro, E. Mattei, E. Pettinelli, GPR detectability of rocks in a Martian-like shallow subsoil: A numerical approach, *Planetary and Space Science* 62(1) (2012) 31–40.
- [15] T. Saarenketo, D. van Deusen, P. Majjala, Minnesota GPR Project 1998: testing ground penetrating radar technology on Minnesota roads and highways, in: D.A. Noon, G.F. Stickley, D. Longstaff (Eds.) *Eighth International Conference on Ground Penetrating Radar*, SPIE, 2000, pp. 396 – 401-396 – 401.

- [16] T. Scullion, T.S. Saarenketo, INTEGRATING GROUND PENETRATING RADAR AND FALLING WEIGHT DEFLECTOMETER TECHNOLOGIES IN PAVEMENT EVALUATION, 2000.
- [17] Y. Mehta, R. Roque, Evaluation of FWD Data for Determination of Layer Moduli of Pavements, *Journal of Materials in Civil Engineering* 15(1) (2003) 25–31.
- [18] W.P.J. van der Meer, Y. Inoue, Using interference to determine the phase change of a reflected GPR pulse, *Proceedings of the Tenth International Conference on Grounds Penetrating Radar, GPR 2004* (2004) 299–302.
- [19] H.M. Jol, *Ground Penetrating Radar Theory and Applications*, Elsevier, Amsterdam, 2009.
- [20] C.W. Chang, C.H. Lin, H.S. Lien, Measurement radius of reinforcing steel bar in concrete using digital image GPR, *Construction and Building Materials* 23(2) (2009) 1057–1063.
- [21] J. Hugenschmidt, A. Kalogeropoulos, The inspection of retaining walls using GPR, *Journal of Applied Geophysics* 67(4) (2009) 335–344.
- [22] J. Hugenschmidt, Concrete bridge inspection with a mobile GPR system, *Construction and Building Materials* 16 (2002) 147–154.
- [23] T.R.D. Souza, Ground penetrating radar as an alternative to radiography, *Insight* 47 (2005) 414–415.
- [24] C. Maierhofer, Nondestructive Evaluation of Concrete Infrastructure with Ground Penetrating Radar, *Journal of Materials in Civil Engineering* 15(3) (2003) 287–297.
- [25] D.H. Chen, T. Scullion, Detecting Subsurface Voids Using Ground-Coupled Penetrating Radar, *Geotechnical Testing Journal* 31(3) (2008) 217–224.
- [26] E. Fisher, G.A. McMechan, A.P. Annan, S.W. Cosway, Examples of reverse-time migration of single-channel, ground-penetrating radar profiles, *Geophysics* 57(4) (1992) 577–586.
- [27] A. Neal, Ground-penetrating radar and its use in sedimentology: Principles, problems and progress, *Earth-Science Reviews* 66 (2004) 261–330.
- [28] F.M. Abdullah, A.A. Al-Shuhail, O.A. Sanuade, Characterization of Subsurface Cavities using Gravity and Ground Penetrating Radar, *Journal of Environmental and Engineering Geophysics* (2019).
- [29] K. Chalikakis, V. Plagnes, R. Guerin, R. Valois, F.P. Bosch, Contribution of geophysical methods to karst-system exploration: an overview, *Hydrogeology journal* 19 (2011) 1169–2011
- [30] S. Lambot, E.C. Slob, I. van den Bosch, B. Stockbroeckx, M. Vanclooster, Modeling of ground-penetrating Radar for accurate characterization of subsurface electric properties, *IEEE Transactions on Geoscience and Remote Sensing* 42 (2004) 2555–2568.
- [31] S. Campana, S. Piro, GPR investigation in different archaeological sites in Tuscany. Analysis and comparison of the obtained results, *Proceedings of the XIII International Conference on Ground Penetrating Radar* (2010) 1–6.
- [32] T. Hao, C.D.F. Rogers, N. Metje, D.N. Chapman, J.M. Muggleton, K.Y. Foo, P. Wang, S.R. Pennock, P.R. Atkins, S.G. Swingle, J. Parker, S.B. Costello, M.P.N. Burrow, J.H. Anspach, R.J. Armitage, A.G. Cohn, K. Goddard, P.L. Lewin, G. Orlando, M.A. Redfern, A.C.D. Royal, A.J. Saul, Condition assessment of the buried utility service infrastructure, *Tunnelling and Underground Space Technology* 28 (2012) 331–344.
- [33] S. Hameda, Geotechnical and geophysical investigation techniques in Ben Ezra Synagogue in Old Cairo area, Egypt, *Heritage Science* 7(1) (2019) 23–23.
- [34] M. Metwaly, Application of GPR technique for subsurface utility mapping: A case study from urban area of Holy Mecca, Saudi Arabia, *Measurement* 60 (2015) 139–145.
- [35] E. Rizzo, L. Capozzoli, G. De Martino, S. Grimaldi, Urban geophysical approach to characterize the subsoil of the main square in San Benedetto del Tronto town (Italy), *Engineering Geology* 257 (2019) 105133–105133.
- [36] K. Knödel, G. Lange, H.-J. Voigt, *Environmental Geology*, Springer Berlin Heidelberg, Berlin, Heidelberg, 2007.
- [37] A.R. von Hippel, S.O. Morgan, *Dielectric Materials and Applications*, *Journal of The Electrochemical Society* 102(3) (1955) 68Ca–68Ca.
- [38] D.S. Parasnis, *Principles of Applied Geophysics*, Springer Netherlands 2012.
- [39] J.M. Reynolds, *An Introduction to Applied and Environmental Geophysics*, Wiley 2011.
- [40] R.A. van Overmeeren, *Georadar for hydrogeology*, 1993.
- [41] I. Møller, F. Jørgensen, *Combined GPR and DC-resistivity imaging in hydrogeological mapping*, 2006.
- [42] H.M. Jol, C.S. Bristow, *GPR in sediments: advice on data collection, basic processing and interpretation, a good practice guide*, *Ground Penetrating Radar in Sediments*, Geological Society of London 2003.
- [43] D.G. Smith, H.M. Jol, Ground penetrating radar: antenna frequencies and maximum probable depths of penetration in Quaternary sediments, *Journal of Applied Geophysics* 33(1) (1995) 93–100.
- [44] M.A.J. Bakker, U.o. London, *The Internal Structure of Pleistocene Push Moraines: A Multidisciplinary Approach with Emphasis on Ground-penetrating Radar*, TNO Built Environment and Geosciences 2004.
- [45] D. Astm, *Standard Guide for Using the Surface Ground Penetrating Radar Method for Subsurface Investigation 1*.